CAPSTONE PROJECT

REPORT ON

DEEP LEARNING BASED HIGH RESOLUTION FOURIER PTYCHOGRAPHY MICROSCOPE

Project Team Members: EIC, 6th SEMESTER

101905032	**Nandini Mohan**
101905037	**Sanya Singh**
101905077	**Nishita Kadian**
101905106	**Diksha Miglani**
101955006	**Yashonidhi Srivastava**

Under the guidance of

Dr. Vishal Srivastava

Assistant Professor, EIED

THAPAR INSTITUTE
OF ENGINEERING & TECHNOLOGY
(Deemed to be University)

Thapar Institute of Engineering and Technology

Electrical & Instrumentation Engineering Department

(Declared as Deemed-to-be-University u/s 3 of the UGC Act., 1956)

Post Bag No. 32, Patiala – 147004

Punjab (India)

TABLE OF CONTENTS

1.1 INTRODUCTION

Fourier ptychography (FP) is a computational imaging technique that offers an effective way to improve the resolution of an imaging system. After acquiring multiple unique images of an object of interest, FP then computationally synthesizes a high-resolution image reconstruction in the Fourier (i.e., spatial frequency) domain. To effectively improve image resolution, FP must convert the multiple intensity images into an estimate of the complex-valued sample, which includes its absorption and phase properties. Unlike holographic approaches, which typically rely on interference with a known reference beam, FP instead solves for the missing phase with an iterative reconstruction algorithm. Accordingly, the technique does not require the reference beam or much additional optical hardware, which makes it particularly well-suited for applications within standard imaging systems. Over the past 6 years, FP has evolved from its first demonstration within a microscope to become a general technique that is now applied in a wide variety of setups and scenarios.

Fourier Ptychographic Microscopy (FPM) offers a way to combine low magnification and high resolution by illuminating the sample off-axis using an LED array. Images captured under illumination at different angles contain information from different regions of the underlying object spectrum. Combining the information contained within the image sequence using iterative phase retrieval allows recovery of a complex image (amplitude and phase) with significantly higher spatial resolution.

Leukaemia is one category of blood cancers that commonly occur in both female and male patients. For the diagnosis and treatment of leukaemia, chromosome karyotyping is critically important; it organizes and pairs all chromosomes in order of decreasing length. In this process, cytogeneticists have to search the whole specimen slide and identify the analyzable metaphase chromosomes, which is a time-intensive and tedious operation. To reduce the clinician's workload and enhance the diagnostic efficiency, many research studies have been focused on the development of automated slide scanners and the associated computer-aided detection schemes, aiming to accomplish quick cell digitization and identification. Despite some encouraging progress, the performance of the current scanners is majorly impeded by the long scanning time, which can be attributed to the limited space-bandwidth product of the objective lens. With few high-cost exceptions, this limitation indicates that it is very difficult for the

objective lens to simultaneously accomplish a large field of view (FOV) and high spatial resolution, which implies that high-resolution objective lenses will have a much smaller FOV than the low-resolution lens. Considering that the chromosome images must be obtained with high spatial resolution to ensure enough details for clinical karyotyping, the corresponding high-magnification scanning will be significantly slower as each acquisition only covers a much smaller area of the specimen.

Meanwhile, the recent technology of Fourier ptychography microscopy (FPM) is an emerging strategy to address the challenge of limited space-bandwidth products. This method first collects a number of low-magnification images under different sample illumination conditions and then synthesizes them together to reconstruct a high-resolution image. Since the data acquisition is under low magnification, it inherits the advantage of low-resolution scanning systems, namely, the large FOV and large depth of field (DOF). For example, in current clinical practice, the 100×/1.25NA100×/1.25 NA objective lens is used to ensure the band pattern sharpness. Given the typical objective lens with an optical field number (OFN) of 22, the corresponding FOV is ∼0.22mm∼0.22 mm. Meanwhile, if FPM is utilized to achieve the same band pattern quality under the 10×/0.25NA10×/0.25 NA lens, the FOV of the objective lens (with the same OFN number) is enhanced to 2.2 mm; thus the scanning efficiency can be greatly enhanced. Moreover, due to the large system DOF, FPM can also vastly reduce the precision requirement of the moving stage, and the total cost of the scanner can be significantly reduced. Although this method has been applied in many different clinical scenarios, no previous research has focused on investigating the feasibility of utilizing FPM on high-resolution metaphase chromosome imaging.

The trade-off between resolution and the imaging field of view is a long-standing problem in traditional imaging systems. This trade-off means an imaging system can produce either an image of a small area with fine details, or an image of a large area with coarse details. Fourier ptychography (FP) is a recently developed approach for tackling this intrinsic trade-off in imaging systems, allowing researchers to have the best of both worlds. It transforms the general challenge of high-throughput and high-resolution imaging from one that is coupled to the physical limitations of optics to one that is solvable through computation. It also provides the ability to computationally correct optical aberrations post-measurement.

The original FP setup1 was modified from an LED-array microscope designed for 3D tomographic imaging2. In this setup, an off-the-shelf LED array is placed beneath a conventional upright microscope with a 2×, 0.08 NA objective lens. The LED array successively illuminates the object from different incident angles. At each angle, the system records a low-resolution intensity image that corresponds to the information from a circular pupil aperture in the Fourier domain . The size of the aperture is determined by the NA of the objective while its offset from the origin is determined by the illumination angle. All captured images are then synthesized in the Fourier domain in an iterative phase retrieval process. The synthesized information in the Fourier domain then generates a high-resolution complex-valued object image that includes both intensity and phase properties. It also retains the original large FOV set by the low-NA objective lens1,3.

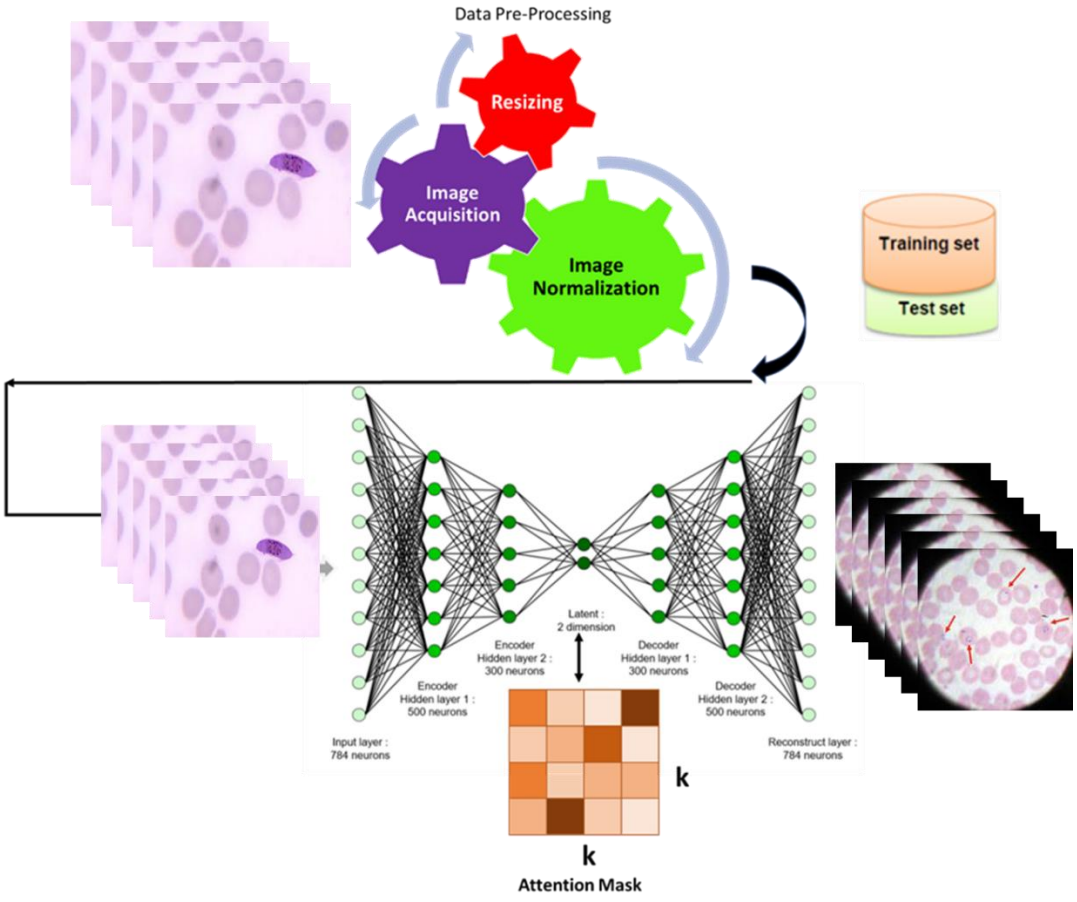

Figure 1.0 Construction of UNET and its application on Malaria Sample

The FP method integrates two innovations in classical optics: synthetic aperture imaging and phase retrieval. Synthetic aperture imaging was first developed at radio wavelengths. It was aimed at bypassing the resolution limit of a single radio telescope by combining images from a collection of telescopes – a feasible task if both phase and intensity information are known. FP employs the same design strategy: synthesizing the pupil aperture at the Fourier plane to bypass the resolution set by the objective lens. With FP, however, no phase is directly measured during the acquisition process, eliminating the challenges of direct phase measurements as in holography. Instead, FP recovers the missing phase from intensity measurements using an iterative phase retrieval process. This process seeks a high-resolution complex-valued object solution that is consistent with many low-resolution intensity measurements. The original FP implementation employed the alternating projection algorithm for recovering the high-resolution complex sample image. In brief, the estimated solution is alternatively projected to two constraint sets in the recovery process. In the spatial domain, the captured images were used as the modulus constraints. In the Fourier domain, the confined pupil apertures were used as the support constraints. Box 1 gives a brief introduction to the alternating projection process with one incident angle, as well as an intuitive explanation about the constraints. For FP, this process is repeated for multiple images captured under different incident angles. The confined pupil aperture, as a result, will be digitally panned across the Fourier space according to the illumination angles, in effect synthesizing a large passband for the complex object.

FP can computationally render both the intensity and the phase images of the sample from intensity-based measurements. FP has the intrinsic ability to computationally correct aberrations. As a result, in FP, the task of aberration correction is not a physical system design problem but, rather, a computational problem that can be resolved post-measurement. Defocus is a type of aberration and, thus, FP can computationally refocus images over a much extended range. Since the invention of FP, various innovations on the original method have been reported; this Technical Review discusses some of the most impactful ones, such as aperture-scanning and camera-scanning schemes, extensions for handling 3D specimens and X-ray FP, among others.

1.2 LITERATURE SURVEY

- FPM (Fourier ptychographic microscopy) is an imaging method which iteratively stitches together many variably illuminated, low resolution intensity images in Fourier space to produce a wide- field, high resolution complex sample image. It can correct for aberrations and digitally extend a microscope's depth of focus beyond the limits of optics. A microscope prototype was built with a half-pitch resolution of 0.78 mm, a field of view of ~120 mm2 and a resolution-invariant depth of focus of 0.3 mm. The Gigapixel color images of histology slides verified its successful operation and the imaging procedure transformed the general challenge of high-throughput, high-resolution microscopy[1].

- FPM is an imaging modality using angularly varying illumination to extend a system's performance beyond the limit defined by its optical components and this technique applies a novel phase-retrieval procedure to achieve resolution enhancement and complex image recovery. FPM data is compared to theoretical prediction and phase-shifting digital holography measurement, showing its acquired phase maps are quantitative and artifact-free. The relationship between the achievable spatial and optical thickness resolution offered by a reconstructed FPM phase image was also explored and was concluded by demonstrating enhanced visualization and collection of unobservable sample information using FPM's quantitative phase[2].

- Embedded pupil function recovery (EPRY) is a pupil function determination algorithm which can be incorporated into the Fourier ptychographic microscopy (FPM) algorithm and recover both the Fourier spectrum of sample and pupil function together. This ERPY-FPM algorithm eliminated the need of previous FPM algorithm for a priori knowledge of aberration in the imaging system to reconstruct a high-quality image. The effectiveness of this algorithm was demonstrated by reconstructing high resolution, large field-of-view images of biological samples. It was illustrated that the pupil function retrieved could be used to study spatially varying aberration of a large field-of-view imaging system, hence this algorithm adds more flexibility to FPM and can be a powerful tool for the characterization of an imaging system's aberration[3].

- This paper presents a method to simultaneously acquire an aberration-corrected, wide field-of-view fluorescence image and a high-resolution coherent bright-field image using a computational microscopy method. First, the procedure applies Fourier ptychographic microscopy (FPM) to retrieve the amplitude and phase of a sample, at a resolution that significantly exceeds the cutoff spatial frequency of the microscope objective lens. Second, the procedure acquires an aberrated fluorescence image, and computationally improves its resolution through deconvolution with the estimated aberration map. An experimental demonstration successfully improves the bright-field resolution of fixed, stained and fluorescently tagged HeLa cells by a factor of 4.9, and reduces the error caused by aberrations in a fluorescence image by up to 31%, over a field of view of 6.2 mm by 9.3 mm. For optimal deconvolution, we show the fluorescence image needs to have a signal-to-noise ratio of at least ~18.

- A method was presented to obtain an aberration-corrected, wide field-of-view fluorescence image and a high-resolution coherent, bright-field image using a computational microscopy method. It applied FPM (Fourier ptychographic method) to retrieve the amplitude and phase of the sample, at a resolution that significantly exceeded the cut off spatial frequency of the microscope objective lens. The demonstration successfully improved the bright-field resolution of fixed, stained and fluorescently tagged HeLa cells by a factor of 4.9, and reduced the error caused by aberrations in a fluorescence image by up to 31%, over a field of view of 6.2 mm by 9.3 mm. It was shown that the fluorescence image needed a signal-to-noise ratio of at least 18 for optimal deconvolution[4].

- From the theoretical analysis of the FPM imaging system, we obtain a preliminary conclusion that the images captured with circular symmetrical illumination angles have no intensity difference when the object is amplitude-only. Considering that FPM uses only intensity images to reconstruct wide-FOV and high-resolution images, we speculate that the images reconstructed with the half number of low-resolution images can attain a comparable resolution to those reconstructed with the whole images in FPM. Owing to the image reduction in this method, the time costs of both image capture and computational processing were reduced by half[5].

- The hardware required was an array of light emitting diodes (LEDs), which was placed several centimeters beneath a thin, semi-transparent sample. This sample was then imaged by a standard microscope using a low-NA objective lens. We will assume that each LED acts as a small point source, and that we turn on just one individual LED in the array to illuminate the sample for the subsequent image formation. Each image is captured with the sample under illumination from a unique angle, ϕ. By shifting the point illumination source to many different positions, it is possible to ensure that a large fraction of the diffracted cone of light passes through the lens and onto the image sensor, albeit at different points in time (i.e., within different images). Fourier ptychography sequentially illuminates the sample from different LEDs within the inserted array, and then computationally merges this data into a single image that appears to have passed through a "synthetic" lens to offer a much higher resolution[6].

- The FP method integrates two innovations in classical optics: synthetic aperture imaging12 and phase retrieval.The method combines images from several telescopes — a feasible task if both phase and intensity information are known.FP recovers the missing phase from intensity measurements using an iterative phase retrieval process (Box 1). This process uses many low-resolution intensity measurements as constraints on a high-resolution, complex-valued object solution[7].

- The FPM curve decreases slowly first and then sharply approaches zero; but the curve of conventional microscopes decreases sharply first and then slowly approaches zero. As a result, at a very wide range of frequency , the FPM microscope can provide better resolving power (i.e., contrast) than the conventional objective lenses, although these two lenses have higher cutoff frequencies.the major advantages of the lens still remain: large FOV and large DOF. This discovery provides a new possible strategy for achieving high-speed chromosome digitization: acquire the raw images under the objective lens and then reconstruct the high-resolution analyzable metaphase chromosomes for the following diagnosis work[8].

- Fourier ptychography (FP) is a computational method for synthesizing raw data into a high-resolution and wide-field-of-view image through a combination of synthetic aperture and phase retrieval concepts. FP can computationally render both the intensity

and the phase images of the sample from intensity-based measurements. FP has the intrinsic ability to computationally correct aberrations. As a result, in FP, the task of aberration correction is not a physical system design problem but, rather, a computational problem that can be resolved post-measurement. Defocus is a type of aberration and, thus, FP can computationally refocus images over a much extended range[9].

- Derived from ptychography, the FPM algorithm shares its roots with phase retrieval and synthetic aperture. The phase retrieval technique leads to a reconstruction of the lost phase information from the measured intensity. And the synthetic aperture combines images from different parts of Fourier space to expand the Fourier passband and improve the achievable resolution. FPM integrates these two aspects and achieves a wide-field, high-resolution reconstruction with quantitative phase [10].

- Unlike the related method of diffraction tomography, FPT just measures normal intensity-only images, and does not need a reference beam to measure phase. This allows FPT to measure very small changes in the index of refraction of primarily transparent samples without using any interferometry (i.e., using a phase-stable laser and a reference beam)[11].

- The light from each angled LED effectively shifts new information emerging from the sample into the microscope lens. The sequence of captured images contains enough information to allow us to computationally recover very high resolution sample features (so far, down to approximately 300 nanometers). We can increase the number of resolvable pixels in an image by a factor of approximately 50-100X, creating some of the first gigapixel images in an imaging system without any moving parts. The technique also increases the microscope working distance and depth-of-field, computationally corrects for system aberrations, and removes the need for oil immersion[12].

References:

1. Zheng, G., Horstmeyer, R., & Yang, C. (2013). Wide-field, high-resolution Fourier ptychographic microscopy. *Nature photonics*, *7*(9), 739-745.
2. Ou, X., Horstmeyer, R., Yang, C., & Zheng, G. (2013). Quantitative phase imaging via Fourier ptychographic microscopy. *Optics letters*, *38*(22), 4845-4848.
3. Xiaoze Ou, Guoan Zheng and Changhuei Yang, "Embedded pupil function recovery for Fourier ptychographic microscopy," Optics Express 22 4960-72 (2014)
4. Jaebum Chung, Jinho Kim, Xiaoze Ou, Roarke Horstmeyer and Changhuei Yang, "Wide field-of-view fluorescence image deconvolution with aberration-estimation from Fourier ptychography," Biomedical Optics Express 7 352-368 (2016)
5. Ao Zhou, Ni Chen1 , Haichao Wang, and Guohai Situ ,"Analysis of Fourier ptychographic microscopy with half of the captured images",J. Opt. 20 (2018) 09570.
6. Pavan Chandra Konda, Lars Loetgering, Kevin C. Zhou, Shiqi Xu, Andrew R. Harvey, and Roarke Horstmeyer," Fourier ptychography: current applications and future promises", Optics Express 9603-9630 (2020)
7. Guoan Zheng, Cheng Shen, Shaowei Jiang, Pengming Song & Changhuei Yang,"Concept, implementations and applications of Fourier ptychography", Nature Reviews Physics volume 3,pages 207–223 (2021).
8. Ke Zhang, Xianglan Lu, Xuxin Chen, Roy Zhang, Kar-Ming Fung, Hong Liu, Bin Zheng, Shibo Li, Yuchen Qiu ,"Using Fourier ptychography microscopy to achieve high-resolution chromosome imaging: an initial evaluation",J. of Biomedical Optics, 27(1), 016504 (2022).
9. Guoan Zheng, Cheng Shen, Shaowei Jiang, Pengming Song & Changhuei Yang,"Concept, implementations and applications of Fourier ptychography", Nature Reviews Physics volume 3,pages 207–223 (2021).
10. Yongbing Zhang, Weixin Jiang, Lei Tian, Laura Waller, and Qionghai Dai,"Self-learning based Fourier ptychographic microscopy",Optics Express,Vol. 23, Issue 14,pp. 18471-18486 (2015).
11. Roarke Horstmeyer, Jaebum Chung, Xiaoze Ou, Guoan Zheng, and Changhuei Yang,"Diffraction tomography with Fourier ptychography",Optica , Vol. 3, Issue 8, pp. 827-835 (2016)
12. Pavan Chandra Konda, Lars Loetgering, Kevin C. Zhou, Shiqi Xu, Andrew R. Harvey, and Roarke Horstmeyer."Fourier ptychography: current applications and future promises",Optics Express Vol. 28, Issue 7, pp. 9603-9630 (2020)

1.3 **NEED ANALYSIS**

1. The existing imaging system can produce either an image of a small area with high resolution or an image of a large area with lower resolution but can hardly achieve both effects simultaneously. Using the proposed methodology, we can produce high intensity images with both a wide field of view and high resolution.

2. The performance of the existing imaging technique is majorly impeded by a prolonged scanning time, which can be caused by the limited space bandwidth product of the objective lens. Fourier Ptychographic Microscopy is a new technique for dealing with the problem of limited space-bandwidth products.

3. The proposed model would be needed massively for automatic quantification of biological cells which can be further utilized for the classification of diseases and profiling. We additionally foresee several applications of the system in the field of research and development as well as testing of novel algorithms.

4. Fourier Ptychography finds major application in the field of aperture scanning and camera scanning on a macroscopic level. The model proposed would provide images with a greater level of intensity which would thereby make the process of Fourier Ptychography highly accurate and detail oriented.

5. Applications such as X-ray and speckle scanning coils benefit largely from the deep learning algorithm that we would implement in terms of the focus to detail with a visible increase in intensity.

1.4 AIM

To design and develop a Fourier Ptychographic Microscope based on a deep learning model.

1.5 OBJECTIVES

1. To design and develop a Fourier Ptychographic Microscope.

2. To develop and integrate the deep learning model with the system to reconstruct high resolution images.

3. To test and experiment the proposed model on red blood cells (RBC) and achieve accurate results with minimal error.

1.6 PROBLEM FORMULATION

There have been several advancements in the field of Fourier Ptychography however, the issue of having a high intensity image only while covering a smaller area seemed to pertain. However, when a larger area was under consideration, the details were rather coarse. Therefore the problem of having a wide view and finer details persisted. We hence propose the following methodology to provide an efficient solution to the issue at hand.

1.7 EXPECTED DELIVERABLES

1. This developed system will be helpful for the automatic quantification of the biological cells with minimal effort and expertise.
2. Further, it will be used for the classification of different diseases related to red blood cells (RBC) like blood cells profiling.
3. The research outcome from the current project will be utilized to further develop and test new and advanced algorithms in the future.
4. Finally, the developed system will be utilized for complete fledge research activities.

1.8 NOVELTY OF WORK

Thus far, all the research work that has been carried out in the area of Fourier Ptychography has largely utilized optical lenses which provide images with a relatively lower resolution than what the application looks for. Hence the novelty of the proposed ideology lies in the fact that a deep learning model will be utilized in lieu of an optical lens which promises to largely increase the intensity since we would be reconstructing several smaller images to obtain a higher resolution.

1.9 PROPOSED METHODOLOGY

Activity 1

- Development of customized deep learning architecture.
- Procurement of material and components.
- Designing of systems.
- Construction of the experimental set-up.
- Synchronization and Experimentation.

Activity 2

- Improvement in the set-up (Hardware & software) if necessary.
- Development of customized deep learning architecture.
- Integration of the network with the developed system
- Optimization of different parameters

1.10 PROPOSED TIMELINE

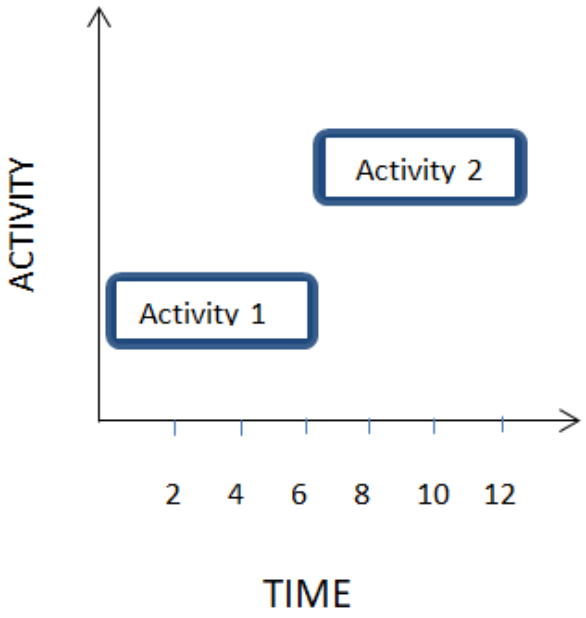

1.10 WORK DISTRIBUTION

S No.	Name	Work Distribution
1	Nandini Mohan	Studying Deep Learning (CNN), Implementation of GAN Network, Construction of UNET, Designing of Fourier Ptychographic Setup and integration of Fourier Ptychographic Setup and UNET
2	Sanya Singh	Studying Deep Learning (CNN), Implementation of GAN Network, Construction of UNET, Designing of Fourier Ptychographic Setup and integration of Fourier Ptychographic Setup and UNET
3	Nishita Kadian	Studying Deep Learning (CNN), Implementation of GAN Network, Construction of UNET, Designing of Fourier Ptychographic Setup and integration of Fourier Ptychographic Setup and UNET
4	Diksha Miglani	Studying Deep Learning (CNN), Implementation of GAN Network, Construction of UNET, Designing of Fourier Ptychographic Setup and integration of Fourier Ptychographic Setup and UNET
5	Yashonidhi Srivastava	Studying Deep Learning (CNN), Implementation of GAN Network, Construction of UNET, Designing of Fourier Ptychographic Setup and integration of Fourier Ptychographic Setup and UNET

CHAPTER 2:

THEORY, STANDARDS AND CONSTRAINTS

2.1. THEORY

2.1.1 THEORETICAL ANALYSIS

To achieve the objective at hand, we employ the following methodologies. We make use of an optical system acts like a low-pass filter, with a cutoff frequency determined by the numerical aperture (NA) of the lens.

Such a low-pass filtering process imposes a resolution limit on the imaging platform.

Following the optical setup, the light signal is sampled by the image sensor. If the pixel size of the image sensor is too large, it would introduce the aliasing problem to the final captured image.

A smaller pixel size of the image sensor helps to address the aliasing problem however, it may also impose limitations on the dynamic range and the signal-to-noise ratio of the sensor chip.

We hence utilise a coherent imaging system where a spatially coherent light source is used for sample illumination. Under coherent illumination condition, the phasor amplitudes of the light field vary in unison at all spatial points.

Coherent illumination condition can be obtained when the light waves come from a single point source. The common light sources for coherent illumination are laser diodes and spatially-confined LEDs.

To simulate the imaging process of a coherent imaging system, we consider a microscope for which we first create a high-resolution input object. We then simulate the low-pass filtering process of the imaging system and ultimately obtain the output complex amplitude and intensity images of the simulated object.

We observe that, a coherent imaging system is linear in complex amplitude, and thus, the

filtering process for the complex amplitude of the light field, not the intensity.

The algorithm switches between the spatial and Fourier domains of the sample estimate. In the spatial domain, the low-resolution intensity measurements are used as object constraints to ensure solution convergence.

2.1.2 WORKING PRINCIPLES

For coherent imaging, the resolution limit for the complex light field is λ/NA, where λ is the wavelength of the incident light.

For incoherent imaging, the resolution limit for the intensity signal is λ/(2NA).

The condition to be satisfied is that the pixel size of the image sensor needs to satisfy the Nyquist limit, i.e., at least two samples are made for the smallest feature of the signal.

A coherent imaging system was utilised where a spatially coherent light source is used for sample illumination. Under coherent illumination condition, the phasor amplitudes of the light field vary in unison at all spatial points.

The recovery process of FP follows the strategy of the phase retrieval technique, seeking a high-resolution sample estimate that is consistent with N low-resolution measurements. Low resolution intensity measurements were utilised in order to ensure the convergence of the images.

2.2. ASSUMPTIONS AND CONSTRAINTS

2.2.1 ASSUMPTIONS

- In the iterative phase retrieval process, the captured images are often segmented into small tiles (Eg. 256 by 256 pixels) for reconstruction. In this way, the pupil aberrations were treated as spatially invariant across the area of each tile, and the LED illumination can be assumed to be planar.

- In the forward imaging model of FP discussed in, the complex object is multiplied with the incident plane wave before passing through the low-pass microscope system. This multiplication process assumes the object section is infinitesimally thin.

- We assume that each LED acts as a small point source, and that we turn on just one individual LED in the array to illuminate the sample for the subsequent image formation.

- We assume the phase of the object is a constant and we convert the intensity to complex amplitude.

- We assume the imaging system does not contain any optical aberration. Such a system is called a diffraction-limited system, where the achievable resolution is only determined by the NA.

- The original FP aberration recovery strategy assumes that the pupil function of the system is fixed during the image acquisition process and does not consider the difference between the pupil aberration and the scannable position in the aperture-scanning FP system, which affects the quality of the reconstructed image to a certain extent.

- The light source in our discussions is assumed to be spatially a point source and temporally a single wavelength. An incoherent mixture of multiple coherent states has not been considered in the FP recovery process.

2.2.2 CONSTRAINTS

- The work also required customized setups and typically imposed additional sample constraints. They did not operate within a standard microscope or connect their reconstruction algorithms to ptychography, from which improvements like computational aberration correction and multiplexed reconstruction may be easily adopted.

- In the spatial domain, the captured images were used as the modulus constraints. In the Fourier domain, the confined pupil apertures were used as the support constraints.

2.3 TECHNICAL STANDARDS

This section briefly discusses the standards used in the project.

- ISO 8036:2015
  Microscopes — Immersion liquids for light microscopy

- ISO 8037-1:1986
  Optics and optical instruments — Microscopes — Slides — Part 1: Dimensions, optical properties and marking

CHAPTER 3

DESIGN METHODOLOGY

3.1. PROPOSED WORKFLOW/ METHODOLOGY

- In the forward imaging model of FP, we capture multiple intensity images of the sample under different incident angles.For this an LED array setup is prepared which will sequentially illuminate the sample with angle-varied plane waves.
- A high-resolution complex image is generated as our input object. We use the ‘camera man’ as the input amplitude and an aerial view image as the input phase, as shown in figure 2.2. The size of the complex input object is 256 by 256.

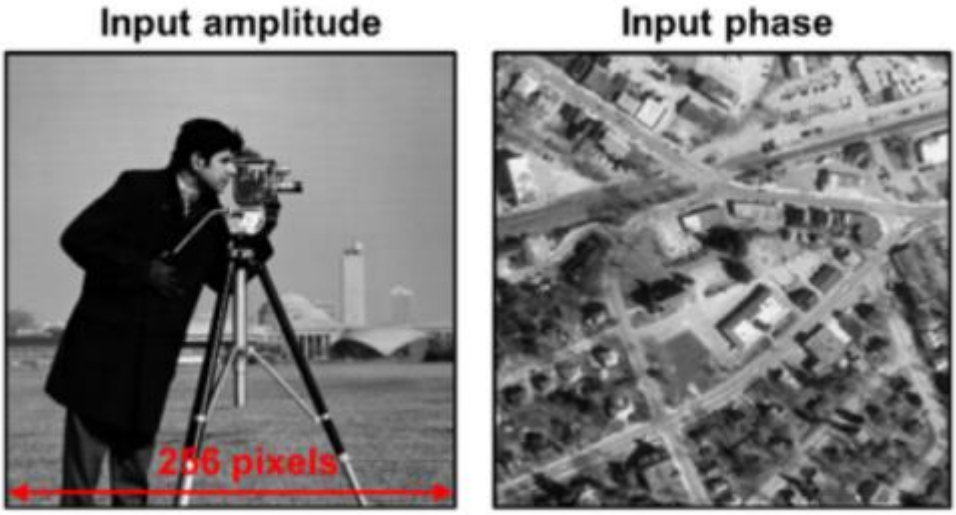

Figure2.2 The simulated input amplitude and phase of the high-resolution object.

- Then we generate the wave vectors for the LED matrix. As shown in figure 2.3, the LED matrix contains 15 by 15 elements. Then we generate the incident wave vectors for the 15 by 15 LED elements, assuming the object is placed at the (0, 0) Position.

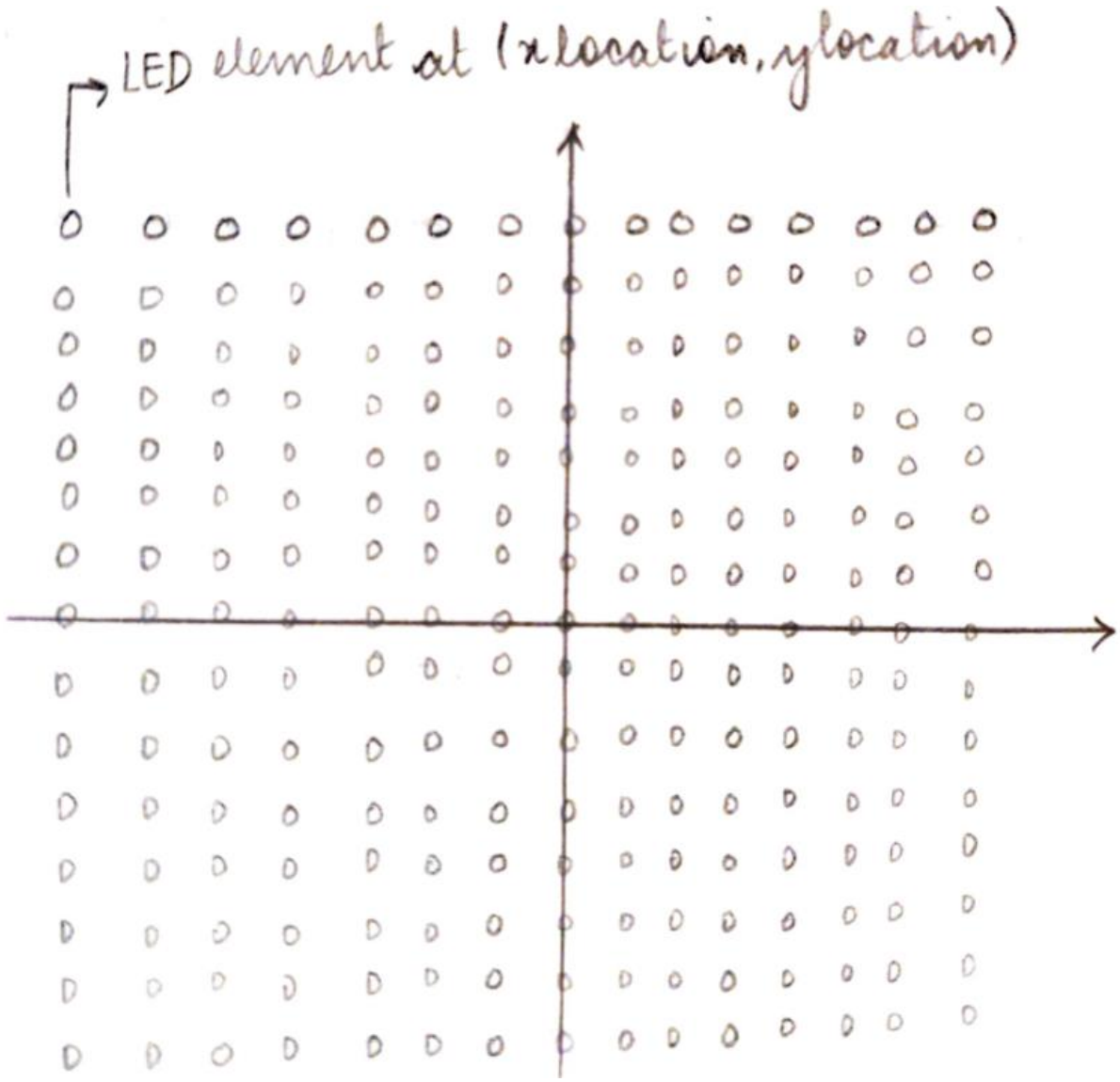

figure 2.3 The LED matrix in the simulation. We use ‘xlocation’ and ‘ylocation’ to determine the position of each LED element. The incident wave vectors can be calculated based on the LED positions.

- Once we generate the wave vectors of the incident waves, we can perform the coherent imaging process. we define the coherent imaging system. In particular, we define two pixel sizes:

    1) the sampling pixel size of the image sensor (i.e. the pixel size of the employed CCD), and
    2) the pixel size of the final reconstructed super-resolution image.

Similarly, we need to deal with two types of image dimensions in this coherent imaging process:

1) the high-resolution input image with a dimension of 256 by 256 pixels, and

2) the low-resolution output with a dimension of 64 by 64 pixels.

we initialize the low-resolution output 'imSeqLowRes', which is an image stack with the dimensions of 64 by 64 by 225.

- In particular, we use 'imSeqLowRes' to store the simulated low-resolution output images corresponding to the 225 different LED elements. we define the coherent transfer function of the coherent imaging system. Then we generate the filtered low-resolution images for different LED elements using.
    - There is a scaling factor which is used to normalize the Fourier magnitude when changing the image size. Then we take the absolute value of the output complex signal, as we lose the phase information in the recording process.
    - Figure 2.4 shows the simulated output images corresponding to the first, the 113, and the 225 LED elements.

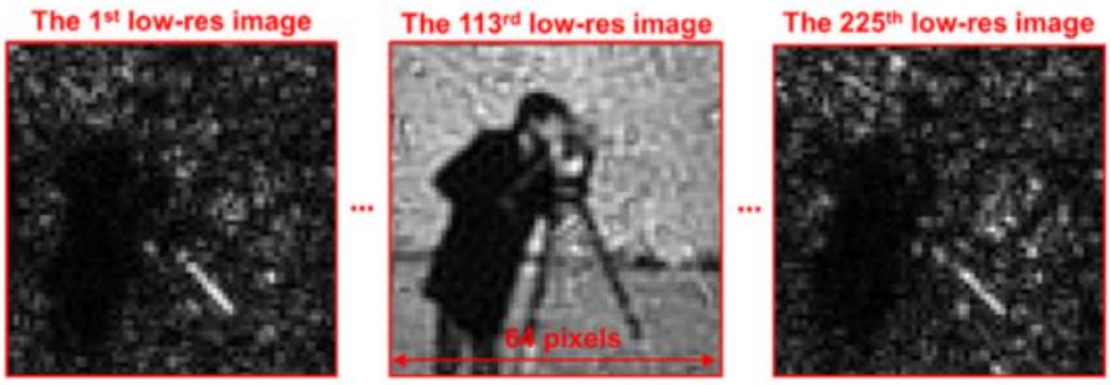

Figure 2.4 The simulated output low-resolution images. These images contain 64 by 64 pixels. The phase information is lost in the recording process.

- We note that, the output image has a dimension of 64 by 64 pixels, 4 times lower than that of the input image in each dimension. The output image only contains the amplitude information, and the phase information is lost in the recording process. The goal of FP is to recover the high-resolution complex object using the low-resolution intensity measurements shown in figure 2.4.

RECOVERY PROCESS

- The recovery process of FP follows the strategy of the phase retrieval technique: seeking a high-resolution sample estimate that is consistent with N low-resolution measurements. The algorithm switches between the spatial and Fourier domains of the sample estimate.
- The FP method makes an initial guess of the high-resolution object in the spatial domain. This initial guess is then transformed to the Fourier domain.
- a small sub-region of the initial guess's Fourier spectrum is selected, equivalent to a low-pass filter of the coherent imaging system, and the inverse Fourier transformation is applied to generate a low-resolution target image . The position of the low-pass filter is selected to correspond to a particular angle of illumination.
- we replace the target image's amplitude with the low-resolution measurement. Then we transform the updated target image back to Fourier domain. The corresponding region of the sample estimate's Fourier spectrum is updated.
- We repeat previous 2 steps for different incident angles. Each shifted sub-region corresponds to a unique, low-resolution intensity measurement and each sub-region must overlap with neighbouring sub-regions to assure convergence. This iterative updating process continues for all N images, at which point the entire high-resolution image in the Fourier space has been modified with all low-resolution intensity measurements.
- At the end of this iterative recovery process, the converged solution in the Fourier space is transformed back to the spatial domain to recover a high-resolution field offering an accurate image of the 2D complex sample with a dramatically increased SBP (high-resolution and wide-FOV).
- Then we use a function 'gseq' to configure the updating sequence of the reconstruction.

Correcting known aberrations in FP

- If the aberration of the system is known, we can model it as a pupil function in the coherent imaging process. We generate a coherent transfer function without aberrations. Then we define a pupil function for defocus aberration and the defocus distance is set to 10 μm. We define the coherent transfer function with the 10-μm-defocus aberration.
- In the forward imaging model of FP, we can then use the aberrated coherent transfer function to perform low-pass filtering and obtain the low-resolution output. Similarly, in the recovery process of FP, we can model and correct for aberrations in each iteration step.
- we generate a low-resolution image using the aberrated coherent transfer function. After that we invert the pupil function to compensate for the known aberration. By simply using these two lines, we are able to model and compensate for any known aberration of the imaging system.

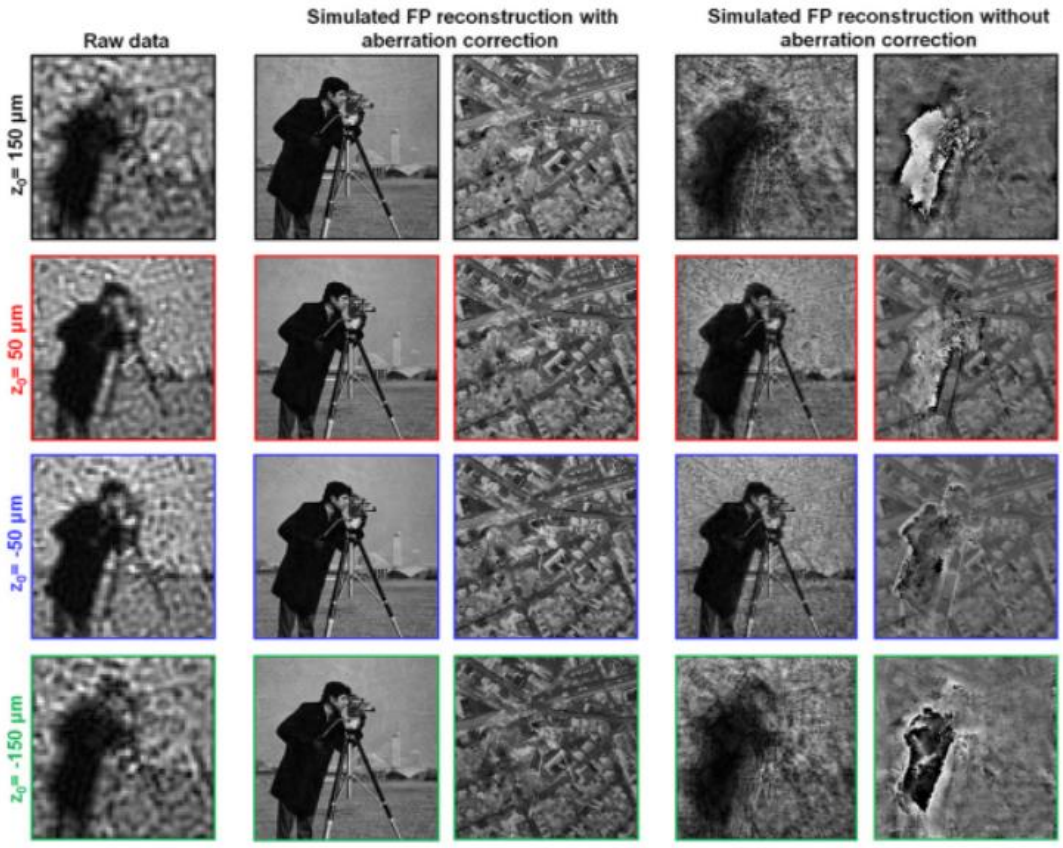

Figure 2.5 Aberration correction in FP.

- We have two approaches for correcting unknown pupil aberrations in FP. The first approach is to use the concepts in adaptive optics for aberration correction and the second approach is to recover both the high-resolution complex object and the unknown aberrated pupil function in the iterative process.
- In this experiment, we used a pathology slide as the sample and a 2×, 0.08 NA objective lens for image acquisition.

Analysing the sampling requirements of FP

- The entire slide was divided into small tiles and the EPRY scheme was applied to each tile to recover both the high-resolution intensity image and the unknown pupil aberration.
- We note that, aperture sizes are different for different colour channels, as they are scaled by different wavelengths and the shape of the pupil function changes from a circle to an ellipse as we move from the centre to the edge of the slide. This is because the 2× objective lens is not a strict telecentric lens and the aperture shape changes asymmetrically as we move towards the edge of the field of view.
- If the aberration is known, we simply invert the pupil function in the iterative process. If the aberration is unknown, we either use the adaptive correction scheme or the EPRY scheme to recover it.

Sampling in the spatial domain

- We use a pixel size of $\lambda/(2 \cdot NA_{obj})$ or smaller to sample the complex signal in the spatial domain. Here, the factor of 2 comes from the Nyquist sampling theorem.
- We divide one original pixel into 4 sub-pixels and the effective pixel size is only half of the original pixel size.
- We then generate a sub-sampled mask in the amplitude updating step .Only 1 out of 4 sub-pixels is updated by the measurement and the other 3 sub-pixels are kept unchanged in the updating process.

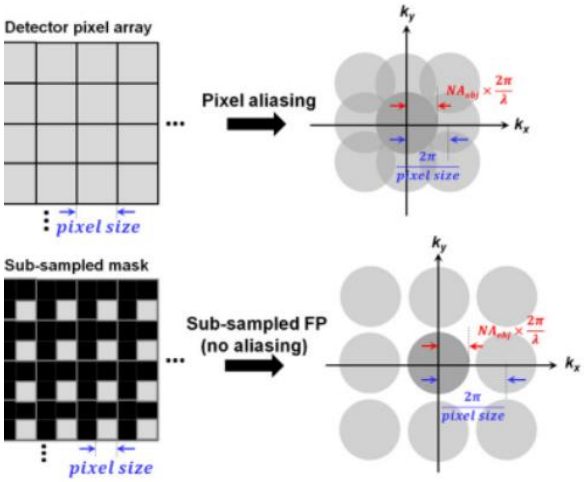

- Each low-resolution image corresponds to a square region in the Fourier space and the final reconstructed images are corrupted by the pixel aliasing problem.
- Due to the limited bit-depth of the image sensors, we acquire multiple images with different exposure times for the same LED element (typically, one short and one long). These raw images are then combined to produce a high-dynamic-range (HDR) image for one LED element.
- In the amplitude updating step, we generate a sparsely sampled mask by binarizing the underexposed/overexposed pixels.
- We then apply the binary mask in the amplitude updating process: the regions with underexposed/ overexposed pixels will be kept unchanged while other regions will be updated by the intensity measurements. As a reference point, the percentage of underexposed/overexposed pixels is typically no more than 15% in an FP experiment.

Sampling in the Fourier domain

- We investigate the spectrum overlapping percentage versus the reconstruction quality. The simulation parameters are chosen to realistically model a light microscope experiment, with an incident wavelength of 632 nm, a pixel size of 2.75 μm and an objective NA of 0.08.
- The RMS error decreases as the overlapping percentage increases, and a minimum of ~35% overlapping percentage is needed for a successful FP reconstruction.

Optimal updating sequence for FP taking the energy criteria

- We design non-uniform sampling patterns for FP by reducing the spectrum overlapping percentage from 40% at the centre (bright-field images) to 15% at the edge (dark-field images).
- Then we consider the following three updating sequences and compare their imaging
- Performances :

  1) a random sequence,

  2) a sequence ranked by the LED illumination NA, and

  3) a sequence ranked by the total energy of the raw images.
- For case 1, we randomly reorder the captured images and use them to update the sample estimate.
- For case 2, we reorder the captured images according to their incident angles (smallest angle ranks first) and update the sample estimate accordingly.
- For case 3, we reorder the captured images according to their total intensity values and update the sample estimate accordingly.

State-multiplexing in FP

- The sample estimate is used to generate multiple low-resolution target images corresponding to different coherent states.
- Second, the intensity components of the target images are summed up to generate
- the incoherent mixture It.
- Third, the ratio between the actual measurement and its used to update the intensity components of the target images, while the phase components are kept unchanged.
- Fourth, the updated target images are used to modify the corresponding spectral regions of the sample estimate.
- Lastly, the entire process is repeated for all intensity measurements with different incident angles and iterated for several times until the solution converges.

- Then we generate the colour object where we set up the coherent imaging system with three different wavelengths and generate the wave vector for the LED array.
- In the forward imaging model, we first generate the three sequences of low resolution images using three coherent transfer functions for different wavelengths. We then incoherently combine these images .
- In the recovery process, we first initialize three high-resolution object images . We generate the incoherent summation of the three coherent states which is then used to update the three coherent states and we then update the high-resolution object images using a similar procedure.
- We also validate the state-multiplexed FP scheme using a light microscope experiment where we use a pathology slide as the sample and turned on R/G/B LEDs simultaneously as the light source. Low-resolution images were acquired using a 0.1 NA objective lens and a monochrome camera.
- We also reconstruct the colour image using three separated FP acquisitions Finally, we note that, the state-multiplexed FP framework is not limited to modelling images at different wavelengths. It can be used to model the partially coherent effect of the employed light source.

3.2. MATHEMATICAL ANALYSIS AND CALCULATIONS

A coherent imaging system is linear in complex amplitude:

$$A_{\text{output}}(x, y) = h(x, y) \otimes A_{\text{input}}(x, y)$$

A_{input} and A_{output} represent the input and output complex amplitudes of the light field, h(x, y) represents the coherent point spread function in the spatial domain, and '⊗' represents 2D convolution.

We can transform the above equation to the spatial-frequency (Fourier) domain and obtain:

$$G_{\text{coh\_output}}(k_x, k_y) = H_{\text{coh}}(k_x, k_y) G_{\text{coh\_input}}(k_x, k_y)$$

Here, G_{coh_input} _ and G_{coh_output} represent the input and output Fourier spectrums of the complex amplitudes. H_{coh} (Kx, Ky) is the Fourier transform of h(x, y) and it is commonly referred to as a coherent transfer function.

In this imaging model of FP, we capture multiple intensity images of the sample under different incident angles. This process can be modeled as a coherent imaging process as follows:

$$A_{\text{output}}(x, y) = h(x, y) \otimes \left(A_{\text{object}}(x, y) e^{ik_{xn}x + ik_{yn}y}\right)$$

We can also transform the above equation to the Fourier domain and obtain:

$$G_{\text{output}}(k_x, k_y) = H_{\text{coh}}(k_x, k_y) G_{\text{object}}(k_x - k_{xn}, \; k_y - k_{yn})$$

We define the image-quality metric of FP as follows:

$$\text{Convergence index} = \sum_{\text{all incident angles}} \frac{\text{mean}(\sqrt{I_l})}{\sum_{x,y} \text{abs}(\sqrt{I_{lm}} - \sqrt{I_l})}$$

where I_1 is the low-resolution target image produced from the sample estimate and I_{lm} is the low-resolution intensity measurement. The 'x-y' summation in the equation is for adding up all the pixel values in the spatial domain, and the 'incident angle' summation is for adding up the contributions of all captured images.

3.3. FLOW CHART

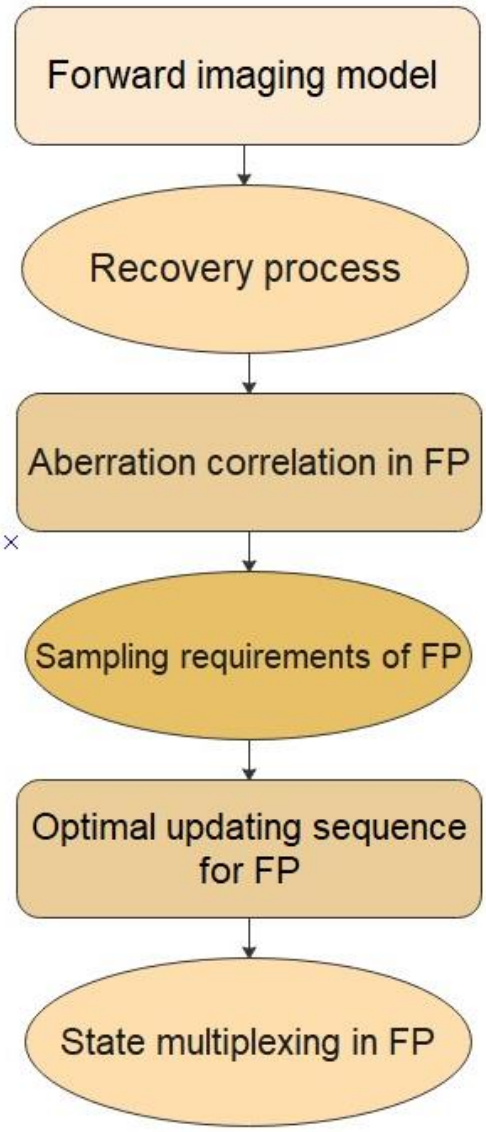

3.4 SIMULATION SETUP

CODE:

```
clc
clear all
close all
objectAmplitude =imread ('cameraman.tif') ;
objectAmplitude=double(objectAmplitude(:,:,1));
phase = double (rgb2gray(imread('img.png')));
phase = pi*imresize (phase, [256 256]) ./max (max
(phase) ) ;
object = objectAmplitude.*exp(1i.* phase);
imshow (abs (object), []);title (' Input complex
object');
arraysize=15;
xlocation=zeros(1,arraysize.^2);
ylocation=zeros(1,arraysize.^2);
LEDgap=4;
LEDheight=90;
for i=1:arraysize
xlocation(1,1+arraysize*(i-1):15+arraysize*(i-
1))=(-(arraysize-1)/2:1:(arraysize-1)/2)*LEDgap;
ylocation(1,1+arraysize*(i-1):15+arraysize*(i-
1))=((arraysize-1)/2-(i-1))*LEDgap;
end;
kx_relative=-sin(atan(xlocation/LEDheight));
ky_relative=-sin(atan(ylocation/LEDheight));

wavelength = 0.63e-6;
k0 =(2*pi)./wavelength;
spsize = 2.75e-6; %% sampling pixel size of the
cCD
psize = spsize / 4; % final pixel size of the
reconstruction
NA = 0.08; %% generate the low-pass filtered
images
[m,n] = size(object); % image size of the high
resolution object
m1 = m/(spsize/psize);
n1= n/ (spsize/psize); % image size of the final
output
imSeqLowRes = zeros (m1, n1, arraysize^2); %
output low-res image sequence
kx = k0 + kx_relative;
ky = k0 * ky_relative;
dkx = 2*pi/ (psize*n);
dky = 2*pi/ (psize*m);
```

```
cutoffFrequency = NA*k0;
kmax=pi/spsize;
[kxm kym] = meshgrid(-kmax:kmax/ ((n1-1)/2) :kmax,
-kmax: kmax/ ( (n1-1) /2) : kmax) ;
CTF = ((kxm.^2+kym.^2) <cutoffFrequency^2); %
coherent transfer function
objectFT =fftshift (fft2 (object) );
for tt=1:arraysize.^2
kxc = round ( (n+1) /2+kx (1, tt) /dkx) ;
kyc = round ((m+1) /2+ky (1, tt) /dky) ;
kyl=round (kyc- (m1-1) /2) ;
kyh=round (kyc+ (m1 -1) /2) ;
kxl=round (kxc- (n1-1) /2) ;
kxh=round (kxc+ (n1-1) /2) ;



imSeqLowFT = (m1/m) ^2 * objectFT (kyl:kyh,
kyl:kyh).*CTF;
imSeqLowRes (:, :,tt) =abs (ifft2 (ifftshift
(imSeqLowFT))) ;
end


figure; imshow (imSeqLowRes (:, :, 100), []);


seq = gseq(arraysize); % define the order of
recovery, we start from the center (the 113rd
image) to the edge of the spectrum (the 225th
image)
objectRecover = ones(m,n);%% initial guess of the
object
objectRecoverFT = fftshift(fft2(objectRecover));
loop=5;
for tt=1:loop
    for i3=1:arraysize^2
        i2=seq(i3);
        kxc =round( (n+1)/2+kx (1,i2)/dkx);
        kyc= round ( (m+1)/2+ky (1,i2)/dky);
        kyl=round (kyc-(m1-1)/2) ;
        kyh=round (kyc+ (m1-1)/2);
        kxl=round (kxc-(n1-1)/2);
        kxh=round (kxc+ (n1-1)/2);
        lowResFT=(m1/m)^2*objectRecoverFT(kyl:
kyh, kyl: kyh).*CTF;
        im_lowRes= ifft2 (ifftshift (lowResFT));
```

```
        im_lowRes =(m/m1)^2*imSeqLowRes
(:,:,i2).*exp(1i.*angle (im_lowRes));
        lowResFT=fftshift (fft2 (im_lowRes)).*CTF;
        objectRecoverFT(kyl: kyh, kyl: kyh)=(1-
CTF).*objectRecoverFT (kyl: kyh, kyl: kyh) +
lowResFT;
     end;
end;
objectRecover=ifft2 (ifftshift (objectRecoverFT));
figure;imshow (abs (objectRecover),
[]);title('test');
figure;imshow (angle (objectRecover), []);
figure; imshow (log (objectRecoverFT), []);


%% page 34-35
cutoffFrequency= NA*k0;
kmax= pi/spsize;
 [kxm kym]=meshgrid(-kmax:kmax/((n1-1)/2):kmax,-
kmax:kmax/((n1-1)/2) :kmax);

CTF=((kxm.^2+kym.^2)<cutoffFrequency^2);
z=10e-6;
kzm=sqrt(k0^2-kxm.^2-kym.^2);
pupil=exp(1i.*z.*real(kzm)).*exp(-
abs(z).*abs(imag(kzm)));
CTF_withaberration=pupil.*CTF;
objectFT=fftshift(fft2(object));
for tt=1:arraysize^2
    kxc=round((n+1)/2+kx(1,tt)/dkx);
    kyc=round((m+1)/2+ky(1,tt)/dky);
    kyl=round(kyc-(m1-1)/2);
    kyh=round(kyc+(m1-1)/2);
    kxl=round(kxc-(n1-1)/2);
    kxh=round(kxc+(n1-1)/2);

imSeqLowFT=(m1/m)^2*objectFT(kyl:kyh,kxl:kxh).*CTF
_withaberration;
    imSeqLowRes(:,:,tt)=
abs(ifft2(ifftshift(imSeqLowFT)));
end;
figure;imshow(imSeqLowRes(:,:,225),[]);
 seq=gseq(arraysize);
 objectRecover=ones(m,n);
 objectRecoverFT=fftshift(fft2(objectRecover));
 loop=5;
 for tt=1:loop
```

```
     for i3=1:arraysize^2
         i2=seq(i3);
         kxc=round((n+1)/2+kx(1,i2)/dkx);
         kyc=round((m+1)/2+ky(1,i2)/dky);
         Kyl=round(kyc-(m1-1)/2);
         kyh=round(kyc+(m1-1)/2);
         kxl=round(kxc-(n1-1)/2);
         kxh=round(kxc+(n1-1)/2);

LowResFT=(ml/m)^2*objectRecoverFT(kyl:kyh,kx1:kxh)
.*CTF.*pupil;
         im_lowRes = ifft2(ifftshift(lowResFT));
         im_lowRes =(m/m1)^2*ImSeqLowRes
(:,:,i2).*exp(li.angle(im_lowRes));
lowResFT=fftshift(fft2(im_lowRes)).*CTF.*(1./pupil
);
objectRecoverFT(kyl: kyh, kxl: kxh)= (1-
CTF).*objectRecoverFT(kyl: kyh, kxl: kxh) +
lowResFT;
 end;
 end;
objectRecover=ifft2(ifftshift(objectRecoverFT));
imshow (abs(objectRecover),[]);

%% page 37
seq=gseq (arraysize);
objectRecover = ones (m, n) ;
objectRecoverFT = fftshift (fft2 (objectRecover));
loop = 5;
converIndex = zeros (loop);
for tt=1:loop
    for i3=l:arraysize^2
        i2=seq (i3);
        kxc = round ((n+1)/2+kx (1,i2)/dkx);
        kyc = round ((m+1)/2+ky (1,i2)/dky);
        Kyl = round (kyc-(m1-1)/2); kyh=round
(kyc+ (m1-1)/2);
        kxl = round (kxc- (n1-1)/2); kxh=round
(kxc+ (n1-1)/2);
        lowResFT = (ml/m)^2*objectRecoverFT (kyl:
kyh, kxl: kxh).*CTF.*pupil;
        im_lowRes = ifft2 (ifftshift (lowResFT));
        converIndex(loop) = converIndex(loop) +
mean(mean(abs(im_lowRes))./sum(sum(abs(im_lowRes
- ImSeqLowRes(:,:,i2))));
        im_lowRes= (m/m1)^2 * ImSeqLowRes (:, :,
i2).*exp(1i.*angle (im_lowRes));
```

```
        lowResFT=fftshift
(fft2(im_lowRes)).*CTF.*(1./pupil);
        objectRecoverFT (kyl: kyh, kxl: kxh) = (1-
CTF).*objectRecoverFT (kyl: kyh, kxl: kxh) +
lowResFT;
    end
end
objectRecover= ifft2 (ifftshift
(objectRecoverFT));

%% page 39
seq = gseq(arraysize);
objectRecover=ones (m, n);
objectRecoverFT=fftshift(fft2(objectRecover));
loop = 25; pupil=1;
for tt=1:loop
    for i3=1:arraysize^2
        i2=seq(i3);
        kxc = round ( (n+1) /2+kx (1, i2) /dkx) ;
        kyc = round ( (m+1) /2+ky (1,i2) /dky) ;
        kyl=round (kyc- (m1 -1) /2); kyh=round
(kyc+ (m1 -1) /2) ;
        kxl=round (kxc- (n1-1)/2) ; kxh=round
(kxc+ (n1-1) /2) ;
        lowResFT_1=(m1/m)^2 * objectRecoverFT(kyl:
kyh, kxl:kxh).*CTF.*pupil;
        im_lowRes = ifft2 (ifftshift
(lowResFT_1));
        im_lowRes=(m/m1)^2 * imSeqLowRes(:, :,
i2).*exp(1i.*angle(im_lowRes));
        lowResFT_2 =fftshift (fft2
(im_lowRes)).*CTF.*(1./pupil) ;
        objectRecoverFT (kyl: kyh, kxl: kxh) =
objectRecoverFT (kyl:kyh, kxl: kxh)+ conj (pupil)
./ (max (max (abs (pupil).^2))).*(lowResFT_2 -
lowResFT_1);
        pupil = pupil +
conj(objectRecoverFT(kyl:kyh,
kxl:kxh))./(max(max(abs(objectRecoverFT(kyl:kyh,
kxl:kxh) ).^2))).* (lowResFT_2- lowResFT_1);
    end;
end;
objectRecover=ifft2 (ifftshift (objectRecoverFT))
;
imshow (abs(objectRecover), []) ;
figure;imshow(angle (objectRecover), []);
figure;imshow(log(objectRecoverFT), []) ;
```

```
%% page 42

seq =gseq(arraysize);
objectRecover = ones (m, n) ;

objectRecoverFT = fftshift (fft2 (objectRecover));

loop =5;

converIndex = zeros (loop);

for tt = 1: loop

for i3 = 1: arraysize ^ 2

i2=seq(i3);

kc = round ( (n+1)/2+kx(1,i2)/dkx) ;

kyc = round((m+1)/2+ky(1,i2)/dky) ;

kyl = round(kyc-(m1-1)/2);kyh= round(kyc + (m1-
1)/2) ;

kxl = round(kxc-(n1-1)/2);kxh h=round(kxc + (n1-
1)/2) ;

lowResFT =(m1/m)^
2*objectRecoverFT(ky1:kyh,kx1:kxh).*CTF.*pupil;

im_lowRes =ifft2(ifftshift (lowResFT));

im_lowRes (1:2:end, 1:2:end) =(m/m1)^ 2*
ImSeqLowRes (:,:,i2).*exp(1i.*angle (im_lowRes));

lowResFT
=fttshift(fft2(im_lowRes)).*CTF.*(1./pupil);

objectRecoverFT (kyl: kyh, kxl: kxh) = (1 -
CTF).*objectRecoverFT (kyl:kyh,kxl:kxh)+lowResFT;

end;

end;

objectRecover = ifft2 (ifftshift
(objectRecoverFT));
```

```
%% page 52

%%simulate the high resolution complex object
im=double (imread ('Lenna.png ' ) ) ;
im=imresize (im, [256 256]) ;
objectAmplitude_r = padarray(im(:,:,1),[128 128]);
objectAmplitude_g = padarray(im (:, :, 2) , [128
128]) ;
objectAmplitude_b = padarray(im (:, : , 3) , [128
128]) ;
phase = double (imread ('westconcordorthophoto.
png'));
phase = imresize (phase, [512 512]) ./max (max
(phase) ) ;
object_r = objectAmplitude_r.*exp (li.* phase) ;
object_g= objectAmplitude_g.*exp (li.* phase) ;
object_b = objectAmplitude_b.*exp (li.* phase) ;
%%setup the parameters for the coherent imaging
system
waveLength_r = 0.63e-6;k0_r = 2*pi/waveLength_r;
waveLength_g = 0.53e-6;k0_g = 2*pi/waveLength_g;
waveLength_b = 0.47e-6;k0_b = 2*pi/waveLength_b;
spsize = 2.5e-6; %%sampling pixel size of the CCD
psize = spsize / 4; %% final pixel size of the
reconstruction
NA=0.1;
%%create the wave vectors for the LED illumination
arraysize=15;
xlocation=zeros (1, arraysize^2) ;
ylocation= zeros (1, arraysize^2) ;
LEDgap = 4;%%4mm between adjacent LEDs
LEDheight = 90; %% distance between the LED matrix
and the sample
for i=1:arraysize%% from top left to bottom right
    xlocation (1, 1+arraysize* (i-1)
:15+arraysize* (i-1)) = (- (arraysize-1) /2:1:
(arraysize-1) /2) *LEDgap;
    ylocation (1, 1+arraysize* (i-1)
:15+arraysize* (i-1)) = ((arraysize-1) /2-(i-1) )
*LEDgap;
end;
kx_relative = -sin (atan (xlocation/LEDheight));

%% 53 LINE 31-92

%% generate the low-pass filtered images
```

```
[m,n] = size (object_r); % image size of high
resolution object
m1= m/(spsize/psize); n1= n/(spsize/psize); %
image size of the output
dkx= 2*pi/(psize*n); dky = 2*pi/ (psize*m);
kmax = pi/spsize;
[kxm, kym] = meshgrid (-kmax: kmax/( (n1-1)/2):
kmax,-kmax:kmax/((n1-1)/2):kmax);
%red channelmatlab: opentoline('/MATLAB
Drive/slide37.m',15,126)
kx_r= k0_r * kx_relative;
ky_r= k0_r * ky_relative;
imSeqLowRes_r = zeros (m1, n1, arraysize^2); % the
final low resolution image sequence
cutoffFrequency_r= NA * k0_r;
CTF_r=
double((kxm.^2+kym.^2)<cutoffFrequency_r^2);
%green channel
kx_g = k0_g * kx_relative;
ky_g = k0_g * ky_relative;
imSeqLowRes_g = zeros (m1, n1, arraysize^2); %the
final low resolution image sequence
cutoffFrequency_g = NA * k0_g;
CTF_g =
double((kxm.^2+kym.^2)<cutoffFrequency_g^2);
%blue channel
kx_b= k0_b * kx_relative;
ky_b= k0_b * ky_relative;
imSeqLowRes_b = zeros (m1, n1, arraysize^2); %the
final low resolution image sequence
cutoffFrequency_b = NA * k0_b;
CTF_b = double ((kxm.^2+kym.^2)
<cutoffFrequency_b^2);
%the incoherent summation of the R, G, B channels
imSeqLowRes= zeros (ml, nl, arraysize^2);
%%forward imaging model
objectFT_r = fftshift (fft2 (object_r));
objectFT_g = fftshift (fft2 (object_g));
objectFT_b = fftshift (fft2 (object_b));
for tt =1:arraysize^2
    %red channel
    kxc_r= round((n+1)/2+kx_r(1,tt)/dkx);
    kyc_r= round ((m+1)/2+ky_r(1,tt)/dky);
    kyl_r = round (kyc_r -(m1-1)/2);
    kyh_r = round (kyc_r +(m1-1)/2);
    kxl_r = round (kxc_r - (n1-1)/2);
    kxh_r = round (kxc_r + (n1-1)/2);
```

```
    imSeqLowFT_r = (m1/m)^2 *
objectFT_r(kyl_r:kyh_r, kxl_r:kxh_r).*CTF_r;
    imSeqLowRes_r(:,:,tt) = abs
(ifft2(ifftshift(imSeqLowFT_r)));
    %green channel
    kxc_g = round ((n+1)/2+kx_g(1, tt)/dkx);
    kyc_g = round ((m+1)/2+ky_g(1, tt)/dky);
    kyl_g = round (kyc_g - (m1-1)/2);
    kyh_g = round (kyc_g + (m1-1)/2);
    kxl_g = round (kxc_g- (n1-1)/2);
    kxh_g = round (kxc_g+ (n1-1)/2);
    imSeqLowFT_g = (ml/m)^2 * objectFT_g (kyl_g:
kyh_g, kxl_g: kxh_g).*CTF_g;
    imSeqLowRes_g(:,:, tt) = abs (ifft2 (ifftshift
(imSeqLowFT_g)));
    %blue channel
    kxc_b = round ((n+1)/2+kx_b (1, tt)/dkx);
    kyc_b = round ((m+1)/2+ky_b (1, tt)/dky);
    kyl_b = round (kyc_b-(m1-1)/2);
    kyh_b = round (kyc_b+ (m1-1)/2);
    kxl_b = round (kxc_b-(n1-1)/2);
    kxh_b = round (kxc_b+ (n1-1)/2);
    imSeqLowFT_b = (ml/m)^2 * objectFT_b (kyl_b:
kyh_b, kxl_b: kxh_b).*CTF_b;
    imSeqLowRes_b(:, :, tt) = abs (ifft2
(ifftshift (imSeqLowFT_b)));
    % summation of R, G, B channels
    imSeqLowRes(:,:,tt) = imSeqLowRes_r(:, :, tt)
+ imSeqLowRes_g(:,:, tt)+ imSeqLowRes_b(:, :, tt);
end
    figure; imshow (imSeqLowRes (:, :,113), []);
%% PAGE 53 LINE
%%Recover the high resolution images at R, G, and
B channels
seq = gseq (arraysize) ;
objectRecover_r= ones (m, n) ;
objectRecoverFT_r = fftshift(fft2
(objectRecover_r));
objectRecover_g = ones (m, n) ;
objectRecoverFT_g = fftshift (fft2
(objectRecover_g));
objectRecover_b=ones (m, n) ;
objectRecoverFT_b = fftshift (fft2
(objectRecover_b)) ;
loop = 25;
for tt=1:loop
    for i3=1:arraysize^2
```

```
        i2=seq(13) ;
    kxc_r=round ((n+1) /2-kx_r (1, i2) /dkx);
    kyc_r=round ((m+1) /2-ky_r (1, i2) /dky) ;
    kxc_g=round ((n+1) /2-kx_g (1, i2) /dkx) ;
    kyc_g=round ((m+1) /2-ky_g (1, i2) /dky) ;
    kxc_b=round ((n+1) /2-kx_b (1, i2) /dkx);
    kyc_b=round ((m+1) /2-ky_b(1, i2) /dky);
    ky1_r= round(kyc_r-(m1-1)/2)
;kyh_r=round(kyc_r+ (m1-1)/2) ;
    ky1_g=round (kyc_g- (m1-1) /2) ;kyh_g=round
(kyc_g+ (m1-1)/2) ;
    ky1_b=round (kyc_b- (m1-1) /2) ;kyh_b=round
(kyc_b+ (m1-1) /2);
    kx1_r=round (kxc_g- (m1-1) /2) ;kxh_r=round
(kxc_r+ (n1-1)/2) ;
    kx1_g=round (kxc_b- (m1-1) /2) ;kxh_g=round
(kxc_g+ (n1-1) /2);
    kx1_b=round (kxc_b- (m1-1) /2) ;kxh_b=round
(kxc_b+ (n1-1) /2);
lowResFT_1r =(m1/m)
^2*objectRecoverFT_r(ky1_r:kyh_r,kxl_r:kxh_r)
.*CTF_r;
lowResFT_1g = (m1/m)
^2*objectRecoverFT_g(ky1_g:kyh_g,kxl_g:kxh_g).*CTF
_g;
lowResFT_1b = (m1/m)
^2*objectRecoverFT_b(ky1_b:kyh_b,
kxl_b:kxh_b).*CTF_b;
im_lowRes_r = ifft2 (ifftshift(lowResFT_1r)) ;
im_lowRes_g = ifft2 (ifftshift (lowResFT_1g)) ;
im_lowRes_b = ifft2 (ifftshift (lowResFT_1b));
rbg_sum =sqrt ( (abs (im_lowRes_r)).^2+(abs
(im_lowRes_g)).^2+(abs (im_lowRes_b)).^2);
im_lowRes_r = (m/m1)^2*imSeqLowRes(:, :,
i2).*abs(im_lowRes_r)./rbg_sum.*exp (1i.*angle
(im_lowRes_r));
lowResFT_2r = fftshift(fft2 (im_lowRes_r) )
.*CTF_r;
im_lowRes_g= (m/m1)^2*imSeqLowRes(:, :, i2).*abs
(im_lowRes_g)./rbg_sum.*exp (1i.*angle
(im_lowRes_g));
lowResFR_2g = fftshift(fft2 (im_lowRes_g) )
.*CTF_g;
im_lowRes_b= (m/m1) ^2 * imSeqLowRes (:, :,
i2).*abs (im_lowRes_b)./rbg_sum.*exp (1i.*angle
(im_lowRes_b));
```

```
lowResFR_2b = fftshift(fft2 (im_lowRes_g) )
.*CTF_b;
objectRecoverFT_r(kyl_r:kyh_r,kxl_r:kxh_r)=objectR
ecoverFT_r(kyl_r:kyh_r,kxl_r:kxh_r)+conj(CTF_r)./(
max(max(abs(CTF_r).^2))).*(lowResFT_2r -
lowResFT_1r);
objectRecoverFT_g(kyl_g:kyh_g,kxl_g:kxh_g)=objectR
ecoverFT_g(kyl_g:kyh_g,kxl_g:kxh_g)+conj(CTF_g)./(
max (max (abs (CTF_g).^2))).* (lowResFT_2g -
lowResFT_1g);
objectRecoverFT_b(kyl_b:kyh_b,kxl_b:kxh_b)=objectR
ecoverFT_b(kyl_b:kyh_b,kxl_b:kxh_b)+conj(CTF_b)./(
max (max (abs (CTF_b).^2))).* (lowResFT_2b -
lowResFT_1b);
    end;
end;
objectRecover_r=ifft2 (ifftshift
(objectRecoverFT_r));
objectRecover_g=ifft2 (ifftshift
(objectRecoverFT_g));
objectRecover_b=ifft2 (ifftshift
(objectRecoverFT_b));
figure; imshow (abs (objectRecover_r), []);
figure; imshow (abs (objectRecover_g), []);
figure; imshow (abs (objectRecover_b), []);
```

SIMULATION: